CIRCULAR ANALYSIS OF GNSS POSITIONING ERROR FOR SHORT-TERM RAPIDLY DEVELOPING IONOSPHERIC STORM SUB-CLASSIFICATION

Lucija Žužić[1,2,*], Ivan Heđi[3], Jonatan Lerga[1,2], Renato Filjar[1,2,4]

[1]University of Rijeka, Faculty of Engineering, Department of Computer Engineering, Rijeka, Croatia
[2]University of Rijeka, Center for Artificial Intelligence and Cybersecurity, Rijeka, Croatia
[3]Virovitica University of Applied Sciences, ICT Department, Virovitica, Croatia
[4]Hrvatsko Zagorje Krapina University of Applied Sciences, Department of Transport Logistics, Krapina, Croatia

*E-mail of corresponding author: lucija.zuzic@uniri.hr

Lucija Žužić 0009-0007-6788-7522, Ivan Heđi 0000-0003-0055-4743,
Jonatan Lerga 0000-0002-4058-8449, Renato Filjar 0000-0002-7040-9931

Resume

In the development of Global Navigation Satellite System (GNSS) Positioning, Navigation, and Timing (PNT), short-lived, fast-growing ionospheric storms (lasting up to three days) were assumed to constitute a single, uniform class of space weather events. To challenge this premise, here is presented a circular analysis of single-frequency commercial-grade Global Positioning System (GPS) horizontal positioning errors in the mid-latitude region during four observed storms (one in 2015 and three in 2017), revealing significant heterogeneity. Maximum positioning errors reached 7.495 m in March 2015, but peaked at 4.261 m, 4.387 m, and 3.948 m during storms in May, early September, and late September 2017, respectively. By demonstrating that short-duration, fast-growing storms require subclassification, in this study is offered a new perspective on disturbances.

Article info

Received 29 April 2026
Accepted 8 July 2026
Online 20 July 2026

Keywords:

GNSS PNT performance
circular analysis
ionospheric correction model
Location-Based Services (LBS)

Available online: https://doi.org/10.26552/com.C.2026.043

ISSN 1335-4205 (print version)
ISSN 2585-7878 (online version)

1 Introduction

Global Navigation Satellite System (GNSS) Positioning, Navigation, and Timing (PNT) services have become essential infrastructure for modern socio-economic applications, yet their performance is highly vulnerable to degradation due to space weather, geomagnetic, and ionospheric dynamics [1-3]. Solar radiation and particle flows from the Sun ionise the Earth's atmosphere, introducing signal propagation delays and GNSS pseudorange measurement errors ($\Delta\vec{\rho}$), that directly propagate into the GNSS positioning error vector ($\Delta\vec{x}$), as given in Equation (1) [4], where G denotes the GNSS Geometric matrix [1-2].

$$\Delta\vec{x} = (G^{\tau}G)^{-1}G^{\tau} \times \Delta\vec{\rho}\,. \tag{1}$$

The GNSS and the quality of PNT services [5] have matured to become essential components of national infrastructure, public goods, and enablers of a vast array of emerging technologies and of the sustainable development of modern economies and societies, as verified by the European Union Agency for the Space Programme (EUSPA) [6].

While the standard models, such as the Klobuchar model, are used to mitigate ionospheric delays, they often leave unmodelled systemic errors during the exceptional space-weather disturbances [7-8]. The Klobuchar model algorithm, which depends on t (local time), with a constant phase offset of $\Phi = 14$ h, is given in Equation (2) for the vertical ionospheric delay (Ion_{VERT}) [8]. Ion_{VERT} is the theoretical delay a signal would experience if the Global Positioning System (GPS) satellite were exactly straight above the receiver [8]. The Direct Current (DC) denotes the constant nighttime ionospheric delay as a baseline offset of 5 ns in the wave function [8]. When the sun is up, solar radiation strongly ionises the atmosphere, and the equation models this as a superimposed half-cosine wave [8].

$$\mathrm{Ion_{VERT}} = \\ = \begin{cases} \mathrm{DC} + \mathrm{A}\cos[2\pi(t-\Phi)/\mathrm{P}](\mathrm{day}) \\ \mathrm{DC};\, if\ \mathrm{A}\cos[2\pi(t-\Phi)/\mathrm{P}] \geq \pi/2\,(\mathrm{night}) \end{cases}. \quad (2)$$

The amplitude A and period P in Equation (3) are given as a function of eight parameters, four pairs of the Klobuchar coefficients $(\alpha_n, \beta_n, n = 0, \ldots, 3)$, broadcast in the GPS and Beidou navigation messages, and the geomagnetic latitude φ [8].

$$A = \sum_{n=0}^{3} \alpha_n \varphi^n; P = \sum_{n=0}^{3} \beta_n \varphi^n . \quad (3)$$

When a signal enters the ionosphere at an angle, it propagates diagonally [8] and therefore the slant ionospheric delay ($\mathrm{Ion_{SLANT}}$), given in Equation (4), is much larger than for the vertical path [8].

$$\mathrm{Ion_{SLANT}} = \mathrm{Ion_{VERT}}\mathrm{m(elev)}. \quad (4)$$

The mapping function m(elev) in Equation (5) represents a geometric multiplier that uses the cosine of the satellite's elevation angle (elev), height of the ionospheric layer (h), and mean radius of the Earth (R_E), which is approximately 6378 km for a spherical model [8]. The height of the ionospheric layer is given as 350 km for GPS and 375 km for Beidou [8]. If a satellite is directly overhead at a 90° elevation, m(elev) is equal to 1 in Equation (5), and $\mathrm{Ion_{SLANT}}$ in Equation (4) is equal to $\mathrm{Ion_{VERT}}$ in Equation (2) [8]. If a satellite is low on the horizon, the mapping function in Equation (5) produces an increased multiplier [8].

$$\mathrm{m(elev)} = [1 - (R_E\cos(\mathrm{elev})/(R_E + h))^2]^{-1/2}. \quad (5)$$

Random errors and unmodelled systemic errors, skewed by exceptional space weather/geomagnetic/ionospheric disturbances, remain mostly uncorrected in the Klobuchar model [7-8], thus providing a significant contribution to the GNSS error budget. Intrinsically, such errors extend the temporal nature that may be explored using circular statistics. Prior studies have identified predictors and target variables (descriptors of geomagnetic, ionospheric, and GNSS PNT conditions) [9] in relation to GNSS PNT accuracy and have examined the impact of geomagnetic storms and solar activity on GNSS signal delays using various modelling and observational approaches. The GNSS systems offer various standard GNSS ionospheric delay estimation (correction) models to mitigate the deteriorating effects on GNSS PNT, such as the Klobuchar model [7, 10]. The standard ionospheric correction models are global and insufficiently flexible in updating and mitigating GNSS ionospheric delay to satisfy rising demands on GNSS PNT performance [10-11].

Analyses of ionospheric effects on the GNSS PNT performance are commonly conducted in terms of specific classes of ionospheric conditions, such as a quiet, mildly, moderately, or considerably disturbed ionosphere. The short-term rapidly-developing ionospheric disturbances [9] are of particular concern for a variety of reasons, including the intensity that causes a significant GNSS PNT performance degradation, and the rapidity that prevents derivation and delivery of suitable GNSS ionospheric corrections to the GNSS users. In the context of this study, a short-term, rapidly developing ionospheric storm is quantitatively defined as a space weather event characterised by a sudden onset and a highly concentrated period of peak intensity that fully resolves within 72 hours (three days). Geophysically, this is typically indicated by a sharp, rapid deterioration in geomagnetic indices (such as a drop in the Disturbance Storm Time (Dst) index below -50 nT or a Planetary K-index (Kp) of 5 or greater within a 12-hour window), accompanied by significant anomalies in the Total Electron Content (TEC) that directly degrade GNSS signal propagation. Still, studies cast doubt on the uniqueness of the short-term, rapidly developing ionospheric disturbance class, thereby precluding consideration of its properties in the development of advanced GNSS ionospheric correction models [9, 12-13].

Here are presented the results of a study aimed at introducing a sub-classification model for short-term, rapidly developing ionospheric disturbances. Using circular statistics applied to experimental GPS horizontal positioning error samples, we identify indicators that characterise the sub-classes of a set of short-term, rapidly-developing ionospheric disturbances, thereby establishing the foundation for bespoke, application-specific scenario-classification-based GNSS ionospheric correction model development [13].

2 Literature review

Previous studies have typically categorised space weather scenarios into broad classes: quiet space weather, moderately disturbed, and strong ionospheric storms. Within these broad definitions, prior research by these authors and others often assumed that short-duration, fast-growing ionospheric storms (lasting up to three days) constituted a single, uniform class. Numerous studies have analysed specific, highly active storm events individually. The four events studied in this paper represent the most significant periods of solar activity in the 24th solar cycle.

For instance, the March 2015 St. Patrick's Day storm from the 17th to the 19th of March 2015 (storm 1) [14-16] has been extensively reviewed with respect to its global multi-instrumental ionospheric response and TEC anomalies [17-18]. Similarly, the intense solar flares and geomagnetic storms of September 2017 (storm 3 from the 7th to the 9th and storm 4 from the 26th to the 28th) have been extensively documented with respect to their effects on ionospheric irregularities [14, 19-20], and GNSS positioning [21-22]. The event from the 27th to the

29th of May 2017 (storm 2) has also been studied using radio and geomagnetic observations [23].

When examining the historical background, previous studies have defined space-weather scenarios into broad categories of quiet space weather, moderately disturbed, and strong ionospheric storms [9]. Prior research, including that by the authors and others [9], assumed that short-duration, fast-growing ionospheric storms constituted a single, uniform class. The primary goal of this study was to challenge the premise of a uniform classification [9]. Recognising that different storms within this group exhibit distinct parameters and characteristics, the research aim was to identify the underlying differences and subcategories within this previously presumed single class [9], to provide new arguments and evidence demonstrating the necessity of a more granular classification system, and to examine how these distinct subclasses specifically affect the quality of GNSS PNT. Prior work shows that adaptive ionospheric models, such as the Satellite-Based Augmentation System (SBAS) and IONosphere Map EXchange (IONEX), can enhance aeroplane position accuracy [24], but they are not locally tuned, which the proposed methodology addresses.

3 Methodology

In the presented research was utilised the circular analysis methodology on a representative dataset of time series of single-frequency commercial-grade horizontal GPS positioning errors, derived from experimental observations in mid-latitude regions during 4 notable ionospheric storms lasting 3 days each, with 1 in 2015 and 3 in 2017. In this Section are outlined the methodology and material used in the presented research.

The standard linear time-series analyses and conventional descriptive statistics are often inadequate for analysing diurnal GNSS error patterns because they fail to account for the continuous, periodic nature of the 24-hour clock. For example, a linear average of error peaks occurring at 23:00 and 01:00 would incorrectly yield a mathematical mean of 12:00 (noon), entirely misrepresenting the data. Circular statistics resolves this boundary issue by mapping the data onto a continuous unit circle, ensuring that the cyclical transition between consecutive days is mathematically preserved. This makes the circular analysis uniquely suited for identifying the true central tendencies and dispersions of daily temporal patterns in ionospheric storm data.

The circular statistics [25] is a separate branch of the discipline of statistics that examines data that can be depicted as points on the circumference of the unit circle. Data of this type is also circular, distinct from the more commonly used linear data. Circular data are represented on the unit circle, analogous to the real line for linear data. In the presented research, the circular data includes directions that represent the hour of the day. Each hour of the day is assigned an angle that defines a point on the circumference of the unit circle, just as each value of a linear variable defines a point on the real line. The hour of the day increases from 0 to 23 in a clockwise direction, starting from the origin, or zero direction, of 90°.

The northing and easting were converted to horizontal positional errors using the International GNSS Service (IGS) [26] station in Sgonico, near Trieste, Italy, with a longitude and latitude of 13.763519885584342°E and 45.70975671789818°N, respectively, as provided by the Metadata Management and Distribution System for Multiple GNSS Networks (M3G) [27].

The circular analysis in the presented research is performed using a tailored software developed by the authors in the open-source R environment for statistical computing, as previously done for the sub-equatorial region [28-29]. The code can be freely downloaded and evaluated from GitHub at https://github.com/LucijaZuzic/circular_trieste.

While the GNSS encompasses multiple constellations, this study focus was on GPS, a foundation for commercial devices, rather than on intersystem issues and associations. The GPS pseudoranges are left uncorrected for ionospheric effects to use as raw material. The RTKLIB Software-Defined Radio (SDR) [30] is configured as a single-frequency commercial-grade GPS receiver and used to post-process pseudorange measurements to obtain estimates of the position components.

The data preparation methodology is described in more detail elsewhere [7]. The RTKLIB software was used in post-processing mode to emulate a typical commercial-grade receiver, using only the GPS L1 C/A pseudoranges, uncorrected for ionospheric effects, to analyse the raw error patterns. The data flow and architecture are depicted using a block diagram in Figure 1.

As shown in Figure 1, after the raw data from the IGS station are processed in RTKLIB [30], the estimated positions are used to compute errors. The resulting time series data is used to study the circular properties of horizontal positioning errors by hour of day in 4 distinct

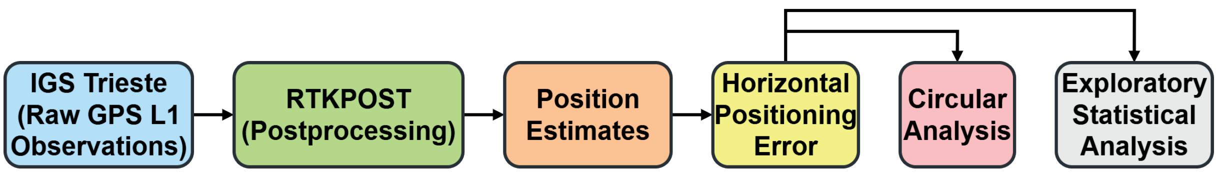

Figure 1 *A data flow and architecture diagram*

events (3 in 2017 and 1 in 2015), each described using 3 days of peak activity. A detailed statistical description, by hour of day, for each event is presented, as well. Horizontal positioning errors are derived using the geodesic distance (the shortest distance on the surface of an ellipsoidal model of the Earth). The default algorithm uses the method proposed by Karney in 2013 [31], which is accurate to round-off and always converges. The material used in the presented research comprises a dataset of horizontal positioning errors obtained from a single-frequency commercial-grade GPS receiver. The GPS-only position estimation process utilises experimental GPS pseudorange observations taken at the IGS reference station in Sgonico, near Trieste, Italy (mid-latitude region, with precisely known position). A 30 s sampling period was used in 2015 and 2017, with a focus on 4 ionospheric events lasting 3 days each.

4 Results

In the presented study are provided the unique insights into the circular features of a representative data set (time series) of single-frequency commercial-grade horizontal GPS positioning errors in mid-latitude regions during four three-day events that represent the most significant periods of ionospheric storms in the 24th solar cycle. In this Section are summarised the results obtained during the conducted research. The circular analysis is analogous to the histogram analysis in classical exploratory statistics. The horizontal positioning errors [m] are divided into five bins of equal size for each hour of the day. This specific number of bins was selected to optimise the balance between the data granularity and visual interpretability within the circular histograms, as utilising fewer bins would oversimplify the data and obscure meaningful structural shifts in the error distribution, whereas utilising more bins would visually clutter the diagrams and hinder the identification of overarching diurnal trends. The circular statistics are supplemented with exploratory statistical analysis of the minimum (min.), 1st quartile (Q_1), median (2nd quartile, Q_2), mean, 3rd quartile (Q_3), maximum (max.), and standard deviation (SD) of the horizontal positioning errors [m] for easier understanding and quantitative support. The lowest Q_1, Q_2, mean, Q_3, and maximum in Table 1 (left) for storm 1 all occurred around 5 o'clock in the morning, as corroborated by Figure 2 (left). Calm periods also include 3 o'clock and 8 o'clock in the morning, as presented in Figure 2 (left), with the lowest standard deviation and minimum in Table 1 (left). On the other hand, the significant disturbances can be observed in Table 1 (left) at 10 o'clock in the morning, with high values for the Q_1, Q_2, and mean. Similar conclusions can be drawn in Table 1 (left) for 17 o'clock in the evening, with high values for the Q_3, maximum, and standard deviation. Finally, the largest of the minimum errors by hour of day in Table 1 (left) occurred around 2 o'clock. The diagram presented in Figure 2 (left) depicts the probability that horizontal GPS errors will appear in the selected range at a certain

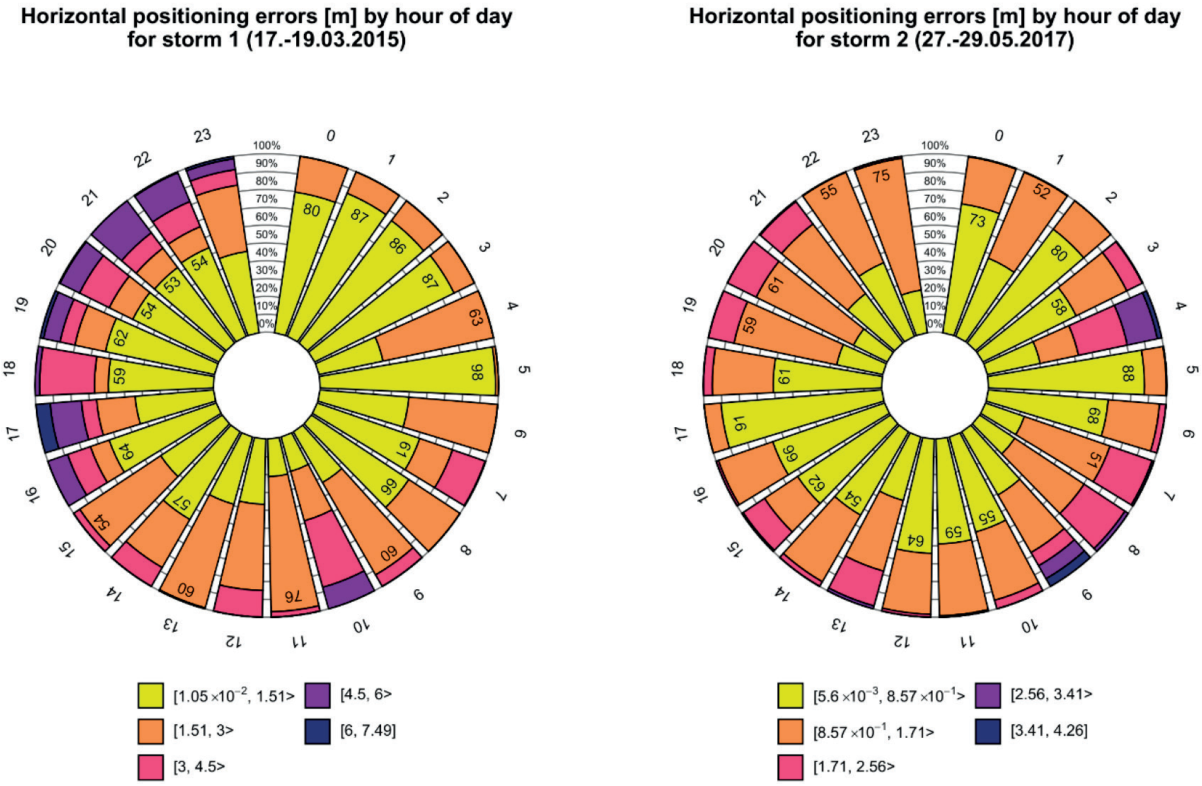

Figure 2 *The horizontal positioning errors [m] by hour of day for storm 1 (left) and storm 2 (right), divided into five equal bins*

Table 1 *The min., Q_1, Q_2, mean, Q_3, max., and SD of the horizontal positioning errors [m] by hour of day for storm 1 and storm 2*

	Storm 1 (17.-19.03.2015)							Storm 2 (27.-29.05.2017)						
Hr	Min.	Q_1	Q_2	Mean	Q_3	Max.	SD	Min.	Q_1	Q_2	Mean	Q_3	Max.	SD
0	0.025	0.66	1.05	1.05	1.43	2.36	0.51	0.056	0.44	0.67	0.68	0.87	1.92	0.31
1	0.095	0.81	1.03	1.09	1.33	2.635	0.43	0.059	0.61	0.87	0.87	1.11	1.722	0.34
2	0.48	0.96	1.15	1.18	1.36	2.147	0.3	0.026	0.44	0.62	0.63	0.82	1.247	0.26
3	0.408	0.99	1.18	1.19	1.37	2.104	0.29	0.067	0.45	0.71	0.87	1.16	2.601	0.56
4	0.398	1.31	1.69	1.69	2.04	2.941	0.53	0.077	0.66	1.59	1.6	2.35	4.186	0.99
5	0.04	0.52	0.77	0.79	1.07	1.699	0.35	0.049	0.24	0.42	0.48	0.67	1.712	0.31
6	0.36	1.1	1.51	1.52	1.91	2.761	0.51	0.042	0.43	0.62	0.73	0.96	2.273	0.43
7	0.169	0.99	1.3	1.73	2.48	4.843	1.05	0.11	0.89	1.38	1.33	1.72	2.718	0.55
8	0.011	0.78	1.27	1.26	1.65	2.743	0.54	0.073	0.91	1.4	1.35	1.8	3.291	0.6
9	0.28	1.3	1.91	1.9	2.48	3.971	0.78	0.042	0.56	1.04	1.27	1.58	4.261	0.95
10	0.077	1.84	3.06	2.87	3.94	5.609	1.36	0.097	0.56	0.8	0.86	1.1	2.383	0.43
11	0.417	1.64	2.26	2.1	2.52	3.503	0.61	0.084	0.53	0.77	0.8	1.01	1.819	0.34
12	0.046	0.96	2.02	1.91	2.71	4.165	1.04	0.035	0.39	0.68	0.74	1.03	2.145	0.43
13	0.037	0.83	1.75	1.55	2.14	3.132	0.76	0.046	0.66	1.03	1.17	1.57	3.18	0.65
14	0.043	0.8	1.36	1.65	2.54	4.3	1.05	0.045	0.5	0.82	0.84	1.14	1.935	0.43
15	0.066	1.09	1.85	1.8	2.47	3.445	0.77	0.027	0.38	0.63	0.87	1.32	2.616	0.65
16	0.109	0.81	1.11	1.92	3.02	5.952	1.6	0.006	0.42	0.68	0.72	0.96	2.185	0.39
17	0.051	1.15	1.7	2.69	4.51	7.495	1.96	0.022	0.37	0.52	0.53	0.69	1.479	0.24
18	0.144	1.03	1.34	2	3.49	5.018	1.31	0.064	0.42	0.7	0.8	1.16	2.255	0.48
19	0.055	0.62	1.09	1.77	2.76	6.51	1.59	0.063	0.83	1.27	1.21	1.58	2.442	0.52
20	0.022	0.83	1.39	2.14	3.68	6.344	1.68	0.154	0.95	1.37	1.29	1.63	2.501	0.48
21	0.233	1.02	1.47	2.36	4.36	5.727	1.74	0.075	0.68	1.08	1.12	1.54	2.668	0.59
22	0.034	0.97	1.41	2.27	4.02	6.119	1.71	0.122	0.69	0.9	0.91	1.12	1.858	0.3
23	0.208	1.17	1.57	1.97	2.24	6.967	1.31	0.123	0.87	1.08	1.07	1.29	1.79	0.3

hour of the day for storm 1. The hours between midnight and 3 o'clock in the morning were not greatly disturbed in Figure 2 (left).

The time between 5 o'clock and 6 o'clock in the morning was the calmest in Figure 2 (left). Undisturbed hours also included 7 and 8 o'clock in the morning and 14 and 16 o'clock in the afternoon in Figure 2 (left). Similar findings were observed between 18 and 22 o'clock in the evening in Figure 2 (left). In contrast, the disturbed hours included 4 o'clock, 9 o'clock, and 11 o'clock in the morning, and 13 and 15 o'clock in the afternoon in Figure 2 (left). The largest percentage of errors between 6 m and 7.49 m occurred around 17 o'clock, as presented in Figure 2 (left).

The lowest Q_1, Q_2, mean, and Q_3 in Table 1 (right) for storm 2 all occurred around 5 o'clock in the morning, as corroborated by Figure 2 (right). Calm periods also include 2 o'clock in the morning, and 16 and 17 o'clock in the evening, as presented in Figure 2 (right), with the lowest maximum, minimum, and standard deviation in Table 1 (right). On the other hand, significant disturbances can be observed at 4 o'clock in the morning in Table 1 (right), with high values for the Q_2, mean, Q_3, and standard deviation. Similar conclusions can be drawn in Table 1 (right) for 20 o'clock in the evening, with high values for the minimum and Q_1. Finally, the largest maximum error occurred around 9 o'clock in Table 1 (right), with a value of 4.261 m. The diagram presented in Figure 2 (right) depicts the probability that horizontal GPS errors will appear in the selected range at a certain hour of the day for storm 2. The hours between 10 o'clock in the morning and noon were not greatly disturbed in Figure 2 (right). The time between 14 o'clock and 18 o'clock in the afternoon was the calmest in Figure 2 (right). Undisturbed hours also included midnight and 2, 3, 5, and 6 o'clock in the morning in Figure 2 (right). The opposite findings were observed between 19 and 20 o'clock in the evening in Figure 2 (right). Continuing in the same fashion, disturbed hours included 1 o'clock and 7 o'clock in the morning, and 22 and 23 o'clock in the evening in Figure 2 (right). The largest percentages of errors between 3.41 m and 4.26 m occurred around 4 o'clock and 9 o'clock in the morning, as presented in Figure 2 (right).

The lowest Q_1, Q_2, mean, and Q_3 in Table 2 (left) for storm 3 all occurred around 1 o'clock in the morning, as corroborated by Figure 3 (left). Calm periods also include 8 and 9 o'clock in the morning, and 16 o'clock in the

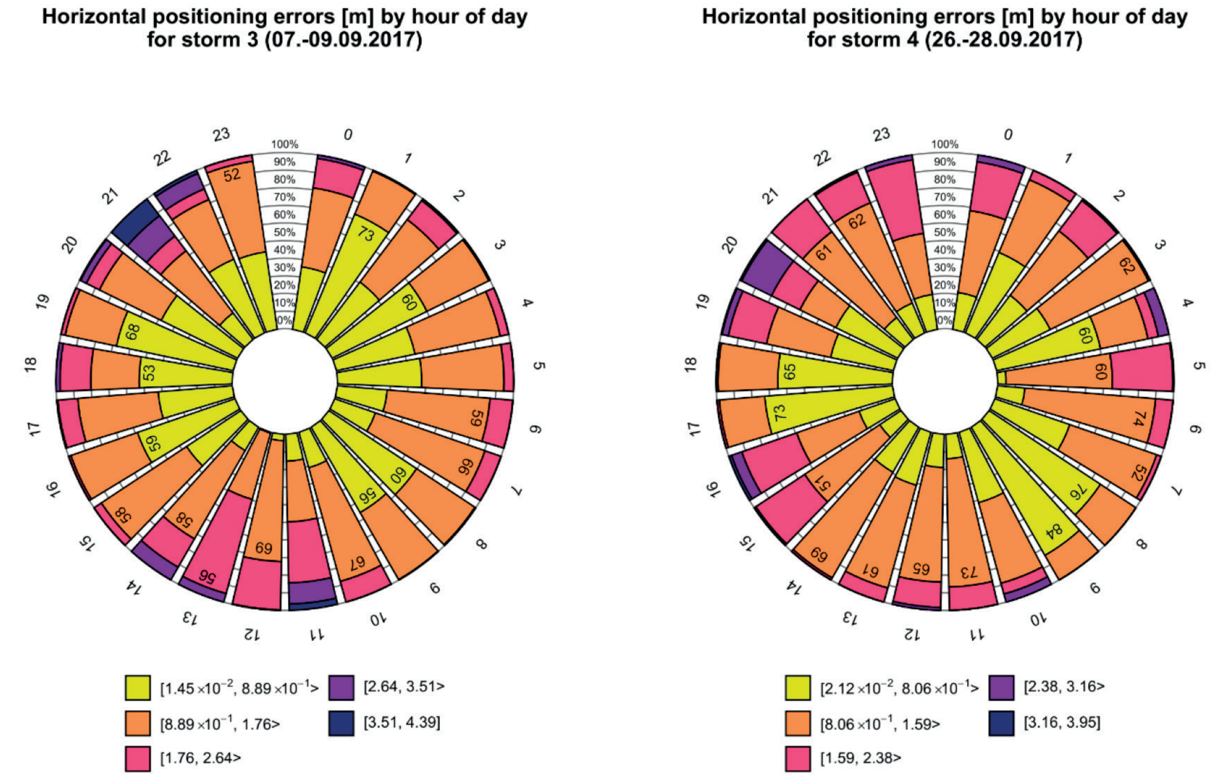

Figure 3 *The horizontal positioning errors [m] by hour of day for storm 3 (left) and storm 4 (right), divided into five equal bins*

evening, as presented in Figure 3 (left), with the lowest maximum, standard deviation, and minimum in Table 2 (left). On the other hand, significant disturbances can be observed at 13 o'clock in the afternoon in Table 2 (left), with high values for the minimum, Q_1, Q_2, and mean. Similar conclusions can be drawn in Table 2 (left) for 21 o'clock in the evening, with high values for the Q_3, maximum and standard deviation. The diagram presented in Figure 3 (left) depicts the probability that horizontal GPS errors will appear in the selected range at a certain hour of the day for storm 3. The hours of 1, 3, 8, and 9 o'clock in the morning were not greatly disturbed in Figure 3 (left). The time between 18 o'clock and 19 o'clock in the afternoon was undisturbed in Figure 3 (left). Undisturbed hours also included 16 o'clock in the afternoon in Figure 3 (left). The opposite findings were observed between 6 and 7 o'clock in the morning in Figure 3 (left). Continuing in the same fashion, disturbed hours included 10 o'clock in the morning, noon, 14 and 15 o'clock in the afternoon, and 23 o'clock in the evening in Figure 3 (left). As many as 56% of the errors were larger than or equal to 1.76 m and smaller than 2.64 m in Figure 3 (left) for 13 o'clock, indicating that there were also disturbances. The largest percentages of errors between 3.51 m and 4.39 m occurred around 11 o'clock in the morning and 21 and 22 o'clock in the evening, as presented in Figure 3 (left). The lowest minimum, Q_1, Q_2, mean, Q_3, maximum, and standard deviation in Table 2 (right) for storm 4 all occurred around 9 o'clock in the morning, as corroborated by Figure 3 (right). However, disturbed periods include 5 o'clock in the morning, noon, and 23 o'clock in the evening, as presented in Figure 3 (right), with the lowest Q_1, mean, minimum, and Q_2 in Table 2 (right).

The significant disturbances can also be observed at 20 o'clock in the evening in Table 2 (right), with high values for the Q_3, maximum, and standard deviation, respectively. The diagram presented in Figure 3 (right) depicts the probability that the horizontal GPS errors will appear in the selected range at a certain hour of the day for storm 4. The hours of 4, 8, and 9 o'clock in the morning were not greatly disturbed in Figure 3 (right). The time between 17 o'clock and 18 o'clock in the afternoon was also calm in Figure 3 (right). However, disturbed hours included 3, 5, 6, and 7 o'clock in the morning in Figure 3 (right). Similar findings were observed between 11 o'clock in the morning and 15 o'clock in the afternoon in Figure 3 (right). Disturbed hours included 21 and 22 o'clock in the evening in Figure 3 (right). The largest percentages of errors between 3.16 m and 3.95 m in Figure 3 (right) occurred around 16 o'clock in the afternoon and 20 o'clock in the evening.

To rigorously validate the visual findings from the circular diagrams and establish empirical boundaries between the subclasses, the inferential circular statistical tests were applied. First, the Rayleigh test for uniformity was conducted on the top quartile of peak errors. The test strongly rejected the null hypothesis of uniformly distributed errors for storm 1, storm 3, and storm 4 (p

***Table 2** The min., Q_1, Q_2, mean, Q_3, max., and SD of the horizontal positioning errors [m] by hour of day for storm 3 and storm 4*

	Storm 3 (07.-09.09.2017)							Storm 4 (26.-28.09.2017)						
Hr	Min.	Q_1	Q_2	Mean	Q_3	Max.	SD	Min.	Q_1	Q_2	Mean	Q_3	Max.	SD
0	0.049	0.67	1.16	1.18	1.59	3.104	0.63	0.191	0.86	1.23	1.32	1.75	3.089	0.58
1	0.025	0.37	0.63	0.67	0.92	2.018	0.39	0.117	0.53	0.81	0.87	1.18	2.131	0.43
2	0.053	0.65	1.05	1.12	1.55	2.886	0.61	0.034	0.64	1.12	1.11	1.49	2.596	0.57
3	0.03	0.52	0.8	0.81	1.04	2.062	0.37	0.112	0.71	0.92	0.92	1.13	1.861	0.33
4	0.101	0.66	0.95	0.99	1.31	2.237	0.44	0.063	0.44	0.65	0.86	1.07	3.038	0.63
5	0.098	0.64	0.91	0.99	1.28	2.427	0.44	0.072	1.18	1.47	1.44	1.68	2.498	0.38
6	0.078	0.85	1.14	1.19	1.52	2.539	0.47	0.128	0.94	1.19	1.17	1.42	1.981	0.35
7	0.309	0.89	1.16	1.2	1.47	2.288	0.41	0.047	0.58	0.86	0.85	1.1	1.911	0.36
8	0.041	0.6	0.82	0.84	1.06	1.945	0.34	0.051	0.46	0.63	0.64	0.79	1.436	0.25
9	0.059	0.6	0.82	0.83	1.05	1.954	0.33	0.021	0.4	0.56	0.57	0.72	1.228	0.23
10	0.124	0.92	1.17	1.21	1.47	2.58	0.43	0.024	0.62	0.88	0.98	1.11	3.079	0.57
11	0.296	1.13	1.78	1.81	2.33	3.982	0.84	0.369	0.94	1.14	1.19	1.46	2.098	0.34
12	0.605	1.21	1.49	1.51	1.8	2.65	0.4	0.378	0.86	1.1	1.19	1.38	2.893	0.46
13	0.792	1.58	1.88	1.89	2.13	3.229	0.43	0.101	0.76	1.01	1.02	1.22	2.303	0.38
14	0.058	1.07	1.43	1.49	1.81	3.467	0.68	0.188	0.78	0.95	0.94	1.1	1.907	0.25
15	0.152	0.73	1.03	1.03	1.28	2.407	0.42	0.157	0.98	1.36	1.35	1.74	2.873	0.48
16	0.015	0.48	0.79	0.8	1.11	2.223	0.41	0.048	0.92	1.46	1.42	1.87	3.893	0.72
17	0.017	0.59	1.03	1.06	1.48	2.888	0.57	0.047	0.42	0.61	0.66	0.83	2.194	0.33
18	0.041	0.53	0.85	1.03	1.47	3.272	0.69	0.024	0.47	0.69	0.71	0.92	1.671	0.33
19	0.037	0.46	0.68	0.76	0.97	2.466	0.42	0.066	0.58	1.11	1.16	1.63	3.274	0.67
20	0.06	0.51	0.91	1.02	1.29	4.069	0.7	0.065	0.47	1.17	1.33	2.19	3.948	0.92
21	0.126	0.99	1.46	1.83	2.73	4.387	1.09	0.3	0.96	1.3	1.27	1.57	2.29	0.41
22	0.04	0.66	0.95	1.23	1.43	3.81	0.86	0.045	0.89	1.12	1.19	1.45	2.512	0.43
23	0.071	0.67	0.97	0.97	1.24	2.216	0.4	0.228	0.9	1.49	1.41	1.87	2.693	0.57

< 0.001), confirming significant directional time-of-day clustering. Interestingly, storm 2 exhibited a much wider dispersion of errors over the 24-hour period, failing to reject the null hypothesis of uniformity at the standard 5% significance level ($p = 0.085$). Subsequent assumption testing revealed low global concentration parameters (kappa < 2), rendering parametric tests for homogeneity of means, such as the Watson-Williams test, statistically inappropriate. Therefore, the non-parametric Mardia-Watson-Wheeler test was utilised to compare the distributions. Due to the high-frequency nature and massive sample size of the GNSS observations, all pairwise non-parametric comparisons yielded highly significant p-values ($p < 0.001$). However, the test statistic (W) quantitatively revealed the underlying subclass structures: the distributional divergence between storm 1 and storm 3 was comparatively minor ($W = 48.5$), whereas comparisons involving storm 2 and storm 4 showed substantial divergence (W ranging from 124.3 to 371.9). Coupled with an analysis of their circular mean vectors, clear practical subclassifications emerge: storm 1 and storm 3 form an afternoon disturbance subclass with peak mean vectors at approximately 15:25 (15.42 h) and 13:56 (13.94 h), respectively. In contrast, storm 2 exhibits a highly dispersed morning tendency (mean vector at 09:18), and storm 4 represents a late-night disturbance subclass with a concentrated peak vector at 21:57 (-2.04 h).

5 Discussion

The circular analysis directly challenges the single-class assumption [9]. Storm 1 (March 2015) exhibited the most severe disturbances, recording a maximum error of 7.495 m around 17 o'clock in the afternoon and a standard deviation and third quartile of 1.96 m and 4.51 m. Its calmest period occurred around 5 o'clock in the morning with a mean error of 0.79 m, and a first quartile, second quartile, third quartile and maximum of 0.52 m, 0.77 m, 1.07 m, and 1.699 m, respectively. In comparison, storm 3 (early September 2017) exhibited its highest error of 4.387 m at 21 o'clock in the evening, also exhibiting a third quartile of 2.73 m and a standard deviation of 1.09 m. Despite the differences in magnitude, the diagrams indicate that storms 1 and 3 share the same subclass.

Conversely, storms 2 and 4 exhibited distinct profiles. Storm 2 (May 2017) exhibited a maximum error of 4.261 m much earlier, around 9 o'clock in the morning. In contrast, storm 4 (late September 2017) peaked at 3.948 m at 20 o'clock in the evening, with a third quartile and standard deviation of 2.19 m and 0.92 m, respectively. These structural and temporal variations in the circular data confirm that storms 2 and 4 each represent completely separate subclasses of short-lived, fast-growing ionospheric storms [9]. The fact that peak errors fluctuate widely between 3.948 m for storm 4 and 7.495 m for storm 1, and that the timing of maximum disturbances shifts dramatically between morning and evening hours, proves that the previously presumed uniform class could be heterogeneous [9].

The inferential statistical analysis provides critical validation for the circular histograms. By demonstrating that the peak temporal distributions occupy distinctly separate diurnal quadrants, such as the afternoon for storms 1 and 3, dispersed morning for storm 2, and late evening for storm 4, the results quantitatively confirm that the presumed uniform class of short-lived, fast-growing ionospheric storms is definitively heterogeneous. The Mardia-Watson-Wheeler test statistics further reinforce this: the relatively low divergence between storms 1 and 3 ($W = 48.5$) supports their grouping into a recurring subclass, while the extreme statistical divergence of storms 2 and 4 ($W > 124$) confirms they represent entirely unique subclasses. Furthermore, the varying degrees of error dispersion, from the highly concentrated nighttime clustering of storm 4 to the near-uniform daily dispersion of storm 2, demonstrate that applying the global, single-model assumptions is inadequate for mitigating the GNSS errors across such events.

6 Conclusion

Identification of indicators extending objectively and measurably the significant differences in the circular diagrams of the examined experimental cases establishes a framework for a more detailed characterisation of short-term, rapidly developing ionospheric storms. Furthermore, in the research is introduced and demonstrated a method for sub-classifying the short-term, rapidly developing ionospheric storms based on circular analysis indicators, thereby enabling the development of bespoke GNSS ionospheric correction models for a more clearly defined class of events affecting GNSS PNT performance. Future research will expand upon this framework by spatio-temporally analysing single-frequency multi-GNSS positioning errors to validate and refine the sub-classification criteria. Identification of single-frequency multi-GNSS positioning performance observed during the short-term, rapidly developing ionospheric storms and disturbances at different latitudes, seasons of the year, and across various systems will render the sub-classification method more generalised and emphasise longer time periods. A validation phase, using independent datasets and comparisons to existing models, is planned to enhance the credibility and applicability. The investigation of underlying physical processes in the ionosphere to link them to statistics and to peak errors in the morning or evening is a primary future objective.

Acknowledgements

This work was supported by the European Regional Development Fund - grant no. PK.1.1.13.0083 and the EU - NextGenerationEU project - grant no. uniri-mzi-25-1 implemented through the University of Rijeka.

Conflicts of interest

The authors declare that they have no known competing financial interests or personal relationships that could have appeared to influence the work reported in this paper.

References

[1] TEUNISSEN, P. J. G., MONTENBRUCK, O. (Eds.). *Springer handbook of global navigation satellite systems* [online] [accessed 2026-07-03]. Chamonix, Switzerland: Springer International Publishing, 2017. ISBN 9783319429281. Available from: https://doi.org/10.1007/978-3-319-42928-1

[2] OXLEY, A. (Ed.). *Uncertainties in GPS positioning: a mathematical discourse* [online] [accessed 2026-07-03]. Amsterdam, Netherlands: Elsevier, 2017. ISBN 9780128095942. Available from: https://doi.org/10.1016/b978-0-12-809594-2.09984-6

[3] DAVIES, K. *Ionospheric radio* [online] [accessed 2026-07-03]. London, UK: IET, 1990. ISBN 9781849193870. Available from: https://doi.org/10.1049/pbew031e

[4] GUSTAFSSON, F. *Statistical sensor fusion*. 3rd ed. Linkoepping, Sweden: Studentlitteratur AB, 2018. ISBN 9789144127248.

[5] SCHAER, S. *Mapping and predicting the earth's ionosphere using the global positioning system*. *Vol. 59* [online] [accessed 2026-07-03]. Zurich, Switzerland: Institute of Geodesy and Photogrammetry, Swiss Federal Institute of Technology, 1999. ISBN 9783908440017. Available from: https://www.sgc.ethz.ch/sgc-volumes/sgk-59.pdf

[6] User needs and requirements - EUSPA [online] [accessed 2026-07-03]. 2024. Available from: https://www.euspa.europa.eu/publications-multimedia/publications/user-needs-and-requirements

[7] KLOBUCHAR, J. Ionospheric time-delay algorithm for single-frequency GPS users. *IEEE Transactions on Aerospace and Electronic Systems* [online]. 1987, **AES-23**(3), p. 325-331 [accessed 2026-07-03]. ISSN 0018-9251. Available from: https://doi.org/10.1109/taes.1987.310829

[8] SANZ SUBIRANA, J., JUAN ZORNOZA, J. M., HERNANDEZ-PAJARES, M. *GNSS data processing, Vol. I: fundamentals and algorithms* [online] [accessed 2026-07-03]. Paris, France: ESA Communications, 2013. ISBN 9789292218867. Available from: https://gssc.esa.int/navipedia/GNSS_Book/ESA_GNSS-Book_TM-23_Vol_I.pdf

[9] LENAC, K., FILJAR, R. Recurrence plot analysis of GPS ionospheric delay time series in extreme ionospheric conditions. *Computers and Geosciences* [online]. 2021, **147**, 104613 [accessed 2026-07-03]. ISSN 0098-3004. Available from: https://doi.org/10.1016/j.cageo.2020.104613

[10] PARKINSON, B. W., SPILKER JR., J. J., AXELRAD, P., ENGE, P. (Eds.). *Global positioning system: theory and applications, 2-volume set* [online] [accessed 2026-07-03]. Washington, DC, USA: AIAA, 1996. ISBN 9781563472497. Available from: https://doi.org/10.2514/4.472497

[11] ENGE, P. K. The global positioning system: signals, measurements, and performance. *International Journal of Wireless Information Networks* [online]. 1994, **1**(2), p. 83-105 [accessed 2026-07-03]. ISSN 1572-8129. Available from: https://doi.org/10.1007/bf02106512

[12] FILIC, M., FILJAR, R. Modelling the connection between GNSS positioning performance degradation, and space weather and ionospheric conditions using RReliefF features selection. In: 31st International Technical Meeting of the Satellite Division of The Institute of Navigation ION GNSS+ 2018: proceedings [online]. 2018. p. 1999-2006 [accessed 2026-07-03]. Available from: https://doi.org/10.33012/2018.16016

[13] FILJAR, R. An application-centred resilient GNSS position estimation algorithm based on positioning environment conditions awareness. In: 2022 International Technical Meeting of The Institute of Navigation: proceedings [online]. 2022. p. 1123-1136 [accessed 2026-07-03]. Available from: https://doi.org/10.33012/2022.18247

[14] CIECKO, A. Analysis of the EGNOS quality parameters during high ionosphere activity. *IET Radar, Sonar and Navigation* [online]. 2019, **13**(7), p. 1131-1139 [accessed 2026-07-03]. ISSN 1751-8792. Available from: https://doi.org/10.1049/iet-rsn.2018.5571

[15] ASTAFYEVA, E., ZAKHARENKOVA, I., FORSTER, M. Ionospheric response to the 2015 St. Patrick's Day storm: a global multi-instrumental overview. *Journal of Geophysical Research: Space Physics* [online]. 2015, **120**(10), p. 9023-9037 [accessed 2026-07-03]. ISSN 2169-9402. Available from: https://doi.org/10.1002/2015JA021629

[16] BENIGUEL, Y., CHERNIAK, I., GARCIA-RIGO, A., HAMEL, P., HERNANDEZ-PAJARES, M., KAMENI, R., KASHCHEYEV, A., KRANKOWSKI, A., MONNERAT, M., NAVA, B., NGAYA, H., ORUS-PEREZ, R., SECRETAN, H., SERANT, D., SCHLUTER, S., WILKEN, V. MONITOR Ionospheric network: two case studies on scintillation and electron content variability. *Annales Geophysicae* [online]. 2017, **35**(3), p. 377-391 [accessed 2026-07-03]. ISSN 1432-0576. Available from: https://doi.org/10.5194/angeo-35-377-2017

[17] MINH, L. H., LAN, T. T., FLEURY, R., AMORY MAZAUDIER, C., THANH, L. T., THANG, N. C., THANH, N. H. TEC variations and ionospheric disturbances during the magnetic storm in March 2015 observed from continuous GPS data in the Southeast Asia region. *Vietnam Journal of Earth Sciences* [online]. 2016, **38**(3), p. 287-305 [accessed 2026-07-03]. ISSN 0866-7187. Available from: https://doi.org/10.15625/0866-7187/38/3/8714

[18] SCOLINI, C., MESSEROTTI, M., POEDTS, S., RODRIGUEZ, L. Halo coronal mass ejections during Solar Cycle 24: reconstruction of the global scenario and geoeffectiveness. *Journal of Space Weather and Space Climate* [online]. 2018, **8**, A09 [accessed 2026-07-03]. ISSN 2115-7251. Available from: https://doi.org/10.1051/swsc/2017046

[19] REDDYBATTULA, K. D., PANDA, S. K., SHARMA, S. K., SINGH, A. K., KURNALA, K., HARITHA, C. S., WUYYURU, S. Anomaly effects of 6-10 September 2017 solar flares on ionospheric total electron content over Saudi Arabian low latitudes. *Acta Astronautica* [online]. 2020, **177**, p. 332-340 [accessed 2026-07-03]. ISSN 0094-5765. Available from: https://doi.org/10.1016/j.actaastro.2020.07.045

[20] ATABATI, A., JAZIREEYAN, I., ALIZADEH, M., PIROOZNIA, M., FLURY, J., SCHUH, H., SOJA, B. Analyzing the ionospheric irregularities caused by the September 2017 geomagnetic storm using ground-based GNSS, swarm, and FORMOSAT-3/COSMIC data near the equatorial ionization anomaly in East Africa. *Remote Sensing* [online]. 2023, **15**(24), 5762 [accessed 2026-07-03]. ISSN 2072-4292. Available from: https://doi.org/10.3390/rs15245762

[21] CIECKO, A., GRUNWALD, G. Klobuchar, NeQuick G, and EGNOS ionospheric models for GPS/EGNOS single-frequency positioning under 6-12 September 2017 space weather events. *Applied Sciences* [online]. 2020, **10**(5), 1553 [accessed 2026-07-03]. ISSN 2076-3417. Available from: https://doi.org/10.3390/app10051553

[22] VANKADARA, R. K., PANDA, S. K., AMORY-MAZAUDIER, C., FLEURY, R., DEVANABOYINA, V. R., PANT, T. K., JAMJAREEGULGARN, P., HAQ, M. A., OKOH, D., SEEMALA, G. K. Signatures of equatorial plasma

bubbles and ionospheric scintillations from magnetometer and GNSS observations in the Indian longitudes during the space weather events of early September 2017. *Remote Sensing* [online]. 2022, **14**(3), 652 [accessed 2026-07-03]. ISSN 2072-4292. Available from: https://doi.org/10.3390/rs14030652

[23] POZOGA, M., MATYJASIAK, B., GRZESIAK, M., ROTHKAEHL, H., PRZEPIORKA, D., WRONOWSKI, R. Observations of the geomagnetic storm 27-28.05.2017 with LOFAR PL610. In: XXXVIII Polish Astronomical Society Meeting: proceedings [online]. Vol 7. 2017. p. 91-93 [accessed 2026-07-03]. Available from: https://w.pta.edu.pl/proc/v7p91

[24] CWIKLAK, J., GRZEGORZEWSKI, M., KRASUSKI, K. Influence of the ionospheric delay on designation of an aircraft position. *Communications - Scientific Letters of the University of Zilina* [online]. 2020, **22**(3), p. 3-10 [accessed 2026-07-03]. ISSN 1335-4205, eISSN 2585-7878. Available from: https://doi.org/10.26552/com.C.2020.3.3-10

[25] PEWSEY, A., NEUHAUSER, M., RUXTON, G. D. *Circular statistics in R*. Oxford, UK: Oxford University Press, 2013. ISBN 9780199671137.

[26] NASA EarthData CDDIS NASA's archive of space geodesy data, open access upon the free registration - NASA [online] [accessed 2026-07-03]. 2026. Available from: https://cddis.nasa.gov/archive/gnss/data/daily

[27] FABIAN, A., BRUYNINX, C., MIGLIO, A., LEGRAND, J. M3G - metadata management and distribution system for multiple GNSS networks [online] [accessed 2026-07-03]. 2021. Available from: https://doi.org/10.24414/ROB-GNSS-M3G

[28] ZUZIC, L., FILJAR, R. Circular analysis of long-term GNSS horizontal positioning error time series observed in the sub-equatorial region. In: 2025 33rd Telecommunications Forum TELFOR: proceedings [online] [accessed 2026-07-03]. 2025. p. 1-4. Available from: https://doi.org/10.1109/telfor67910.2025.11314378

[29] R: A language and environment for statistical computing - R Core Team [online] [accessed 2026-07-03]. 2026. Available from: https://www.r-project.org

[30] TAKASU, T. RTKLIB: an open source program package for GNSS positioning, ver. demo5 b34k [online] [accessed 2026-07-03]. 2024. Available from: https://github.com/rtklibexplorer/RTKLIB/releases

[31] KARNEY, C. F. F. Algorithms for geodesics. *Journal of Geodesy* [online]. 2013, **87**(1), p. 43-55 [accessed 2026-07-03]. ISSN 1432-1394. Available from: https://doi.org/10.1007/s00190-012-0578-z